NIH Public Access
Author Manuscript
J Magn Reson Imaging. Author manuscript; available in PMC 2010 October 1.

Published in final edited form as:
J Magn Reson Imaging. 2009 October ; 30(4): 743–752. doi:10.1002/jmri.21908.

Improving Dynamic Susceptibility Contrast MRI Measurement of Quantitative Cerebral Blood Flow using Corrections for Partial Volume and Nonlinear Contrast Relaxivity: a Xenon CT Comparative Study

Greg Zaharchuk, PhD, MD[1], **Roland Bammer, PhD**[1], **Matus Straka, PhD**[1], **Rexford D Newbould, PhD**[2], **Jarrett Rosenberg, PhD**[1], **Jean-Marc Olivot, MD, PhD**[3], **Michael Mlynash, MD, MS**[3], **Maarten G Lansberg, MD, PhD**[3], **Neil E Schwartz, MD, PhD**[3], **Michael M Marks, MD**[1], **Gregory W Albers, MD**[3], and **Michael E Moseley, PhD**[1]

[1]Department of Radiology, Stanford University, Stanford, CA, USA

[2]Clinical Imaging Centre, GlaxoSmithKline, London, UK

[3]Stanford Stroke Center, Department of Neurology and Neurological Sciences, Stanford University Medical Center, Stanford, CA, USA

Abstract

Purpose—To test whether dynamic susceptibility contrast MRI-based CBF measurements are improved with arterial input function (AIF) partial volume (PV) and nonlinear contrast relaxivity correction, using a gold-standard CBF method, xenon computed tomography (xeCT).

Materials and Methods—18 patients with cerebrovascular disease underwent xeCT and MRI within 36 hrs. PV was measured as the ratio of the area under the AIF and the venous output function (VOF) concentration curves. A correction was applied to account for the nonlinear relaxivity of bulk blood (BB). Mean CBF was measured with both techniques and regression analyses both within and between patients were performed.

Results—Mean xeCT CBF was 43.3±13.7 ml/100g/min (mean±SD). BB correction decreased CBF by a factor of 4.7±0.4, but did not affect precision. The least-biased CBF measurement was with BB but without PV correction (45.8±17.2 ml/100 g/min, coefficient of variation [COV]=32%). Precision improved with PV correction, although absolute CBF was mildly underestimated (34.3±10.8 ml/100 g/min, COV=27%). Between patients correlation was moderate even with both corrections (R=0.53).

Conclusion—Corrections for AIF PV and nonlinear BB relaxivity improve bolus MRI-based CBF maps. However, there remain challenges given the moderate between-patient correlation, which limit diagnostic confidence of such measurements in individual patients.

Keywords

magnetic resonance imaging; perfusion; computed tomography; xenon CT; cerebral blood flow; quantitation; stroke; cerebrovascular disease; dynamic susceptibility contrast

Please address correspondence to: Greg Zaharchuk, Ph.D., M.D., 1201 Welch Rd., Mailcode 5488, Stanford, CA 94305-5488, tel: 650-723-5393; fax: 650-723-9222; gregz@stanford.edu.

NIH-PA Author Manuscript
NIH-PA Author Manuscript
NIH-PA Author Manuscript

NIH-PA Author Manuscript

NIH-PA Author Manuscript

NIH-PA Author Manuscript

Introduction

Bolus dynamic susceptibility contrast (DSC) MRI provides important information about brain hemodynamics, such as relative cerebral blood volume (CBV), mean transit time (MTT), and cerebral blood flow (CBF) (1,2). Østergaard et al. laid the theoretical groundwork for non-parametric CBF measurement using singular value decomposition(3) and demonstrated good concordance between spin-echo echo planar imaging (EPI) DSC and $H_2{}^{15}O$ PET in 6 normal subjects (4). Further studies using gradient echo (GRE) EPI also found reasonable correlations in individual subjects, but the scaling factor between DSC and gold standard CBF measurements differed between subjects (5-7). This has led many to conclude that DSC CBF measurements are not reliable (8-10), and indeed clinical DSC MRI is generally evaluated qualitatively only. It would be preferable to measure quantitative CBF, as the need for some interventions is predicated on patient-specific absolute CBF measurements (11). Also, absolute CBF measurements would be useful to evaluate whole brain disease.

There are several reasons why DSC CBF measurements are unreliable. Some errors are global (i.e., uncertainty about the relationship between tracer concentration and measured relaxivity, the effects of large and small vessel hematocrit, etc.), while others are patient specific (i.e., related to cardiac output, arterial input function [AIF] and venous output function [VOF] orientation and signal saturation, etc.). Patient specific errors can be further broken down into those that affect the amplitude of the AIF, VOF, and tissue concentration curves, such as choices of scaling coefficients for relaxivity and AIF partial volume (PV), and those that lead to shape changes (12). In the AIF, shape errors arise from either signal saturation to noise levels, signal intensity changes due to vessel orientation (13), and distortion due to inclusion of surrounding brain tissue (5,14). Additionally, recent studies suggests that contrast relaxivity for voxels composed mainly of blood (“bulk blood” or BB) has a quadratic rather than linear dependence with concentration (13,15,16). This would alter the relative concentration relationship between the AIF and tissue, and significantly decrease quantitative DSC CBF measurements (17). The goal of this study was to determine how corrections for BB and PV affect the bias and precision of DSC CBF measurements, using stable xenon computed tomography (xeCT) as a gold standard. We have chosen to focus on conventional gradient echo EPI DSC, since this is still the most common method used in clinical practice.

Materials and Methods

Patient population

The study was approved by the Institutional Review Board and was HIPAA compliant. Patients were enrolled if they had symptoms consistent with cerebral ischemia (acute, subacute, or chronic) or transient ischemic attack (TIA), and signed written prior informed consent to participate in the study. Exclusion criteria was a level of consciousness score of 2 or greater as defined by the National Institutes of Health stroke scale; symptoms likely related to psychoactive drugs or patients with symptoms related to an active inflammatory disease such as AIDS, meningitis, or cerebritis; psychiatric or substance abuse disorder or dementia that interfered with evaluation or interpretation of the neurologic and mental assessment; severe coexisting or terminal systemic disease that limited life expectancy or otherwise interfered with the conduct of the study; symptoms related to an alternative diagnosis such as seizures or migraine; or use of any thrombolytic agent or acute stroke investigational drug therapy. Patients were recruited between October 2004 and July 2008.

Eighteen patients (9 men, 9 women; mean age 47±17 yrs, range 19-87 yrs) with cerebrovascular disease (4 acute stroke, 6 subacute stroke, 2 TIA, 6 Moyamoya; of these, 6

NIH-PA Author Manuscript

NIH-PA Author Manuscript

NIH-PA Author Manuscript

had unilateral internal carotid (ICA) occlusion, while 2 had bilateral ICA occlusion) were enrolled in the study and underwent both xeCT and MRI CBF measurements. The mean time difference between the two examinations was 18±10 hrs with a range of -21 to +34 hrs). In 6/18 patients, the MRI study preceded the xeCT study. Diffusion positive lesions representing acute or early subacute cerebral ischemia were seen in 9 of 18 patients (50%). Table 1 describes the demographics of the patients included in the study.

xeCT CBF

Computed tomography (CT) was performed using a GE Lightspeed 8 detector scanner integrated with a stable xenon enhancer system (Diversified Diagnostic Products, Houston, TX, USA). The xeCT protocol imaged 4 contiguous 10 mm slices (80 kVp, 240 mA) with the lowest slice at the level of the basal ganglia. 8 sets of images were acquired at 45 s intervals. The first 2 timepoints were acquired during room air inhalation, while the remaining 6 timepoints were acquired during 28% Xe gas inhalation. End-tidal Xe concentration was assumed equal to arterial Xe concentration, a reasonable approximation except in patients with severe respiratory disease. CBF was calculated using the Kety autoradiographic method by the manufacturer's commercial software according to reference (18), yielding CBF maps with a nominal in-plane 1 mm spatial resolution. The true in-plane resolution is on the order of 2-3 mm, and all image calculations (see below) were performed on regions-of-interest (ROI's) measuring 10 × 10 mm in-plane.

Dynamic susceptibility contrast MRI

MRI scans were performed at 1.5T (Signa LX/i, GE Medical Systems, Waukesha, WI, USA). Anatomic imaging was performed in addition to DSC, and always included fluid-attenuated inversion recovery (FLAIR) and diffusion-weighted imaging (DWI) with an isotropic b-value of 1000 s/mm^2. DSC was performed using GRE EPI with the following parameters: 12 slices, thickness 7.5 mm, FOV 24 cm, flip angle 60°, TR/TE 2000/60 ms, matrix 128×128, 40 cine time points. A power injector was used to inject 20 ml of either gadopentetate dimeglumine or gadodiamide followed by 20 ml saline at a rate of 4 ml/s.

CBF maps were created using a block-circulant (delay-insensitive) singular value decomposition (SVD) in line with the work of Wu et al. (19). Transverse relaxivity change (ΔR2*) was calculated using:

$$\Delta R2^*(t) = \frac{-\ln\left(S(t)/S_0\right)}{TE} \quad [1]$$

where S_0 is the mean signal intensity before contrast, excluding the first 3 time points to ensure a steady-state value. To avoid subjective selection of AIF and VOF, we employed automatic selection, based on location, peak value, peak width, and contrast arrival time (20,21). 10 voxels were used for the AIF and VOF ROIs (17). This algorithm resulted in AIF locations in middle cerebral arteries, anterior cerebral arteries, basilar artery, or ICAs. The VOF locations were typically in the superior sagittal sinus, transverse sinus, or straight sinus. We did not account for possible clipping of the AIF or VOF curves due to MR signal saturation. In our experience, it is difficult to determine the presence of saturation based purely on shape, in accordance with theoretical work (14).

Four separate post-processing corrections were applied to the DSC CBF maps: no corrections, PV correction only, BB correction only, and both PV and BB corrections. PV was defined as the ratio of the area under the AIF and the VOF curves (Figure 1), using trapezoidal integration. These timecurves were sampled over the entire scanning period,

NIH-PA Author Manuscript

NIH-PA Author Manuscript

NIH-PA Author Manuscript

with only the post-contrast segment contributing to the area (as the mean tracer concentration before bolus arrival is by definition zero). Corrections for the BB quadratic relaxivity relationship (described below) were applied before deconvolution. Given the linear relationship between the AIF underestimation and CBF (22), the DSC CBF maps were multiplied by the PV level in each patient, such that PV correction led to reduced CBF.

BB correction was performed according to references (13,15,16). For the uncorrected images, a linear relationship between relaxivity and concentration was used for both the tissue and vessels (AIF and VOF) (13,15):

$$c(t)=\frac{\Delta R2^*(t)}{r} \quad [2]$$

where r = 0.044 (ms mM)$^{-1}$. For the BB corrected maps, a quadratic relationship was used for the AIF and VOF (13):

$$\Delta R2^*(t)=ac(t)+bc(t)^2 \quad [3]$$

where a = 7.6 × 10^{-3} (ms mM)$^{-1}$ and b = 574 × 10^{-6} (ms mM^2)$^{-1}$, while the linear relationship in Eq. 2 was applied for tissue. BB correction leads to a relative increase in the estimated AIF concentration, resulting in decreased calculated CBF.

Within patients CBF measurements

Rigid body rotation based on mutual information using SPM2 (University College of London, available at www.fil.ion.ucl.ac.uk/spm/software/spm2) was used to co-register the MR and CT images. A 1 × 1 cm square grid were laid over each of the 4 slices, resulting in about 125 individual 1 cc ROIs per slice, such that each patient's mean CBF measurement was calculated as the mean of about 500 small cubic ROIs. Voxels belonging to the ventricles and cortical sulcal CSF were excluded by manual thresholding the diffusion-weighted images. In each patient, scatterplots of the individual DSC and xeCT CBF ROI yielded slope, intercept, and correlation coefficient.

Between patients CBF measurements

To compare between patients, we chose to examine the global CBF, which we define as the mean CBF of all voxels within the co-registered volumes, as this will be independent of intrinsic spatial resolution. It should be noted that this represents a subset of the entire MR CBF dataset, since it covered a larger volume of brain than the xeCT measurements. For each patient, this yielded a single xeCT measurement and 4 separate DSC measurements, corresponding to each of the correction methods described above. To compare the two measurements, the CBF ratio was used:

$$CBF\ ratio=\frac{DSC\ CBF_{mean}}{xeCT\ CBF_{mean}} \quad [4]$$

Ideally, this value should be 1, representing exact correspondence (i.e., no bias) between the two techniques.

NIH-PA Author Manuscript

NIH-PA Author Manuscript

NIH-PA Author Manuscript

Once the CBF ratios for each of the post-processing conditions were calculated for each patient, comparisons between patients were performed. The precision of the measurement was measured using the coefficient of variation (COV), also known as the normalized between-patients standard deviation:

$$COV = \frac{SD_{CBF\ ratio}}{mean_{CBF\ ratio}} = \frac{\sqrt{\sum_n (CBF\ ratio_n - \overline{CBF\ ratio})^2/(n-1)}}{\overline{CBF\ ratio}} \quad [5]$$

where the overbar represents the mean of all patients. A low COV represents a more precise measurement. Finally, linear regression was performed between the xeCT and each of the separate DSC CBF measurements.

Statistical Analysis

Bland-Altman plots were created using the xeCT CBF (gold standard) measurement as the x-axis. Mean difference and 95% limits of agreement are reported. To assess for possible bias in the measurement based upon underlying xeCT CBF, we created rank-ordered maps. To test the significance of the global xeCT and various MRI-based CBF measurements in different patients, we have calculated the simple Pearson correlation coefficient and the corresponding p-value.

Results

Mean xeCT CBF was 43.3±13.7 ml/100 g/min. The nine diffusion positive patients all had regions of decreased xeCT CBF, except for one patient, who had elevated CBF in the DWI-positive region, presumably representing reperfusion of a completed infarct. With the exception of 1 case with very low CBF (20.0 ml/100 g/min in an 87 year old man with a subacute infarct) and 1 case with markedly increased CBF (81.1 ml/100 g/min in a 19 year old man with subacute bacterial endocarditis), the xeCT CBF values were clustered around the 40-55 ml/100 g/min range.

Within patients CBF analysis

A typical example of a co-registered data set is shown as Figure 2. Correlation between all of the MRI DSC correction approaches and the xeCT CBF was significant ($p<0.05$) in individual patients, with correlation coefficients ranging between 0.15 and 0.64 (Table 2). There was no difference between the mean correlation coefficients with or without BB correction (with BB correction: 0.40±0.15; without BB correction 0.41±0.15). Correlation did not change based on PV correction, as this resulted in only global CBF changes. Also, the slopes on average did not converge around 1 and the intercepts did not go through 0 (and were in fact always positive). An example of the correlation between xeCT and DSC in an individual patient is shown as Figure 3.

Between patients CBF analysis

The PV of the AIF ranged between 0.49 and 1.0, with a mean value of 0.78±0.15. In two cases, the area under the VOF was smaller than that under the AIF (patients #15 and #16, where the AIF area divided by the VOF area was 1.10 and 1.30, respectively); in both cases, this was due to a higher post-contrast baseline for the AIF compared with the VOF, and the PV was set to 1 in these cases (Figure 4). Bulk blood correction decreased DSC CBF by an average factor of 4.7±0.4.

NIH-PA Author Manuscript

NIH-PA Author Manuscript

NIH-PA Author Manuscript

Global MRI-based CBF ranged between 34.3±10.8 ml/ 100 g/min (both PV and BB correction) and 211.9±73.9 ml/100 g/min (no corrections) (Table 3). The maps with BB but without PV correction had the least bias, overestimating xeCT CBF by 7±34%, while the maps with both PV and BB correction led to underestimation (-19±22%). The COV ranged between 27% and 33%, with the PV corrected maps having the best precision. The best correlations (R=0.52-0.53, $p<0.05$) were seen after BB correction, which were higher than those seen with either no corrections (R=0.45, p=0.06) or with PV correction alone (R=0.42, p=0.08). Bland-Altman plots for the different MR correction methods are shown as Figure 5. Figure 6 plots the BB corrected MRI-based CBF values versus the xeCT gold standard measurement, and demonstrates the effect of the PV correction.

Discussion

Accurate CBF measurement in clinical patients with cerebrovascular disease remains a serious imaging challenge. Quantitative CBF may be useful to weigh the risks and benefits of surgical versus medical management (11). This frequently necessitates more invasive imaging tests, such as stable xeCT, $H_2{}^{15}O$ PET, or single photon emission tomography, occasionally requiring patients to be imaged at specialized centers distant from their usual outpatient or inpatient setting. Both CT and MR bolus brain perfusion measurements have been criticized as inaccurate, particularly in the setting of large vessel disease, due to regional delay and dispersion of the bolus (23-25). Other errors that impact DSC measurements surround accurate measurement of contrast concentration in the AIF and tissue (16,26). While some of these problems may be mitigated by the use of parallel and/or multiecho approaches (17), single shot GRE EPI is by far the most common implementation in clinical practice. This paper addresses how correction for AIF partial volume and differences in relative contrast relaxivity between large vessels and tissue affect DSC CBF measurements, using a diffusible tracer method as a gold-standard.

Partial volume corrections

It is critical to accurately determine the contrast concentrations within the AIF and the tissue, as inaccuracies in either of these will cause CBF errors due to the scaling of the tissue residue function using the SVD methodology (22). Tracer kinetic theory states that the area under the concentration-time curve of a ROI consisting completely of blood should be equal regardless of location. Since veins tend to be larger than arteries, the ROI used to define the VOF is more likely to contain 100% blood, and thus the ratio of AIF and VOF timecurves is a reasonable approach to measure PV. We have chosen to integrate the AIF and VOF over the entire time period following the bolus arrival. This leads to a slight overestimation of the PV ratio, since the AIF precedes the VOF by several seconds. Thus, the true VOF integrated area (for equal recirculation times) will be underestimated. However, since the late recirculation part of both the arterial and venous curves is low compared with area contained in the peak, we estimate that this error is small, likely less than 5%. Since this is far smaller than the interpatient variability in PV (15%) and not particularly patient-dependent, we have neglected it in the calculations. Finally, we wish to emphasize that the approach described above can only correct for amplitude effects, and cannot address potential shape errors (14).

Applying this amplitude PV correction reduced DSC CBF by 22% and improved precision, as evidenced by the drop in the COV measurement, though the bias of the measurement became negative (i.e., the PV and BB corrected maps underestimated true CBF as measured by xeCT). Thus, the PV correction is partially effective in alleviating the patient-to-patient variation in CBF. However, it is important to realize that even after correction, the scatter of DSC CBF measurements compared with xeCT CBF is 27% of the mean. Of course, all measurement methods, xeCT included, will have an underlying variation, which should be considered when determining whether the variation seen in the DSC measurements is

NIH-PA Author Manuscript

NIH-PA Author Manuscript

NIH-PA Author Manuscript

clinically acceptable. Test-retest measurements could be used to address this question, though the radiation associated with xeCT makes such studies problematic.

Other groups have recognized the importance of PV errors in quantitative DSC CBF measurements. Østergaard et al. studied 6 pigs with DSC and PET (27), and normalized the AIF area by the injected dose on a weight basis, determining a global scaling factor by requiring that the MR and PET measurements be equal. This is equivalent to assuming that the percent of the cardiac output to the brain is uniform among subjects. After this correction, they reported a spread of slopes in the individual correlations of about 10%. Another approach was suggested by Lin et al. (5), who applied a patient-specific correction factor based on the ratio of the VOF area with an average value found in a small series of normal volunteers. Using this method, they report a decrease in the spread in the slopes of individual patient data, with overall improved correlation. It is unclear why this method improves precision, given that it does not address the fundamental issue of the PV error associated with the AIF. They comment that they evaluated a procedure similar to that in the current study for normalization, but that it was not effective. A study of normal subjects using a ^{133}Xe SPECT gold standard (28) used a similar correction strategy to that used in the current study, and found improved correlation, though no data regarding the COV of the CBF ratios were reported.

Bulk blood non-linear relaxivity correction

Previous DSC studies have reported elevated CBF levels compared with both gold standard (5,7,8,28) and literature values (17,29,30). For example, the study of Jochimsen et al. measured approximately 4-fold increased CBF compared with literature estimates, even after potential problems with T1 relaxivity and AIF dynamic range were addressed using a parallel multiecho approach (17). One possible explanation is that the standard assumption that contrast relaxivity is a linear function of concentration is flawed. Kiselev (15) suggested that there is a quadratic relationship between relaxivity and concentration in blood-filled voxels. van Osch et al. (13) demonstrated such a nonlinear relationship in experiments on *ex vivo* human blood.

Correcting for this effect markedly decreased MRI-based CBF measurements, bringing the values into the range of those measured with xeCT. This correction is, in theory, patient dependent, due to the influence of the quadratic relationship on the amplitude of the patient's AIF (which itself is due to the underlying partial volume and the fractional cardiac output that goes to the brain). However, since the peak AIF concentrations in the different patients were similar, this had a smaller effect on the patient-to-patient basis than the PV correction. Thus, including this factor significantly improved the bias of the measurement, but did not improve precision. It should be noted that the coefficients used in the quadratic correction (Eq 3) were obtained from blood *in vitro* and might be different *in vivo*. We also neglected the possible changes in the coefficients that might be related to hematocrit, which could also presumably differ in gray and white matter (26). Finally, theoretical and experimental considerations suggest that vessel orientation with respect to the main magnetic field may play a significant role in the relationship between relaxivity and concentration as well as on AIF shape (14,31,32), which we did not address (14).

Both the PV and BB correction are problematic in the setting where the peak concentrations of the AIF and VOF are underestimated due to the inherent noise floor of the measurement, a particular concern for GRE EPI sequences with relatively long echo times. We observed some degree of plateau-like appearance to the AIF and VOF concentration time curves in 3 and 9 patients, respectively. Signal clipping is a known problem, which is inherent to single-echo GRE-EPI acquisitions with reasonably long TE. However, for typical injection rates (4 ml/s), clipping at the peak of AIF and VOF can appear even with shorter TE, at which point

NIH-PA Author Manuscript

NIH-PA Author Manuscript

NIH-PA Author Manuscript

the SNR of the measurement is compromised. Multiecho approaches, such as PERMEATE (33), may alleviate some of these issues. Such errors would likely cause CBF overestimation, though no obvious trend towards CBF overestimation was seen in these patients.

Correlations within and between individuals

Instead of manually choosing ROIs on the xeCT and DSC maps, we divided the 4 imaged brain slices of the xeCT into cubic 1 cc regions, excluding the ventricular system and other CSF spaces. This method eliminates potential bias in ROI selection, and uniformly samples the entire co-registered volume, enabling a straightforward measurement of mean CBF. With this approach, we observed marked variation in slopes, intercepts, and correlation coefficients between DSC and xeCT CBF values (Table 2). This finding is consistent with prior studies that have not used *post hoc* correction schemes (4-6).

When between-patient correlations between DSC and xeCT are examined, a similar trend emerges. While correction for PV and BB improves the correlation between the two techniques, it is still only moderate at best, and significant variation remains even with both corrections. This remains a significant barrier to clinician confidence in individualized measurements. In our institution, when absolute CBF levels are critical for patient care, xeCT is performed despite the inconvenience and radiation dose.

Limitations of the current study

Comparing DSC to xeCT CBF is fraught with several difficulties. xeCT is a diffusible tracer method, while DSC relies on intravascular tracers. In particular, the gradient echo implementation is particularly sensitive to large blood vessels (Figure 3). This was particularly problematic in the setting of focal ischemia, where vasodilation in the periphery tended to decrease conspicuity of low CBF regions in the core. Since vessel size is a continuum, defining a precise threshold for the removal of large vessels is problematic; for this reason, we chose not to attempt to remove large vessels *post hoc*. It is possible that spin-echo DSC or arterial spin labeling (ASL), each of which are less sensitive to large vessel effects, may offer improved CBF measurements. Difficulties with spin-echo DSC include the need for increased contrast dose and questions surrounding how to measure the AIF concentration. Conventional ASL is hampered by transit delay times caused by stenotic vessels or anastomoses and more advanced ASL methods are warranted. Also, we did not account for possible effects of vessel orientation upon the relationship between measured transverse relaxivity and contrast concentration (14), as the automated method used criteria based solely on peak height, narrowness, and early arrival. Future studies could evaluate the effect of choosing a standard AIF location.

The patient population studied had cerebrovascular disease, as this is a common indication for DSC perfusion imaging. Many had arterial occlusions or stenoses that would lead to spatially dependent delay and dispersion. Block-circulant SVD is accurate in the setting of delay, but not dispersion (19). Local AIF approaches may decrease the effects of delay and dispersion by choosing more proximal AIFs for each voxel (34). However, AIFs in smaller vessels are more susceptible to PV artifacts. While both studies were acquired within 36 hrs, true CBF changes between the two timepoints may also serve to decrease correlations between the two techniques. CBF has a daily variation of about 10% and can be affected by medication and diet, which were not controlled for in this study. Some prior studies suggest that xenon inhalation itself causes a small CBF increase (35,36). Though these patients were deemed to have stable physiology, CBF changes related to disease course are possible. Finally, given the challenge of acquiring acute xeCT and the associated radiation, the sample size is relatively small.

NIH-PA Author Manuscript

NIH-PA Author Manuscript

NIH-PA Author Manuscript

In conclusion, corrections for partial volume and nonlinear contrast relaxivity improve the bias and precision of DSC measurements compared with a gold standard CBF measurement in patients with cerebrovascular disease. After these corrections, DSC maps still mildly underestimate xeCT CBF, have about 27% patient-to-patient variability, and are only moderately correlated with xeCT CBF. These factors limit diagnostic confidence of quantitative DSC CBF measurements in individual patients using current methodology. Further refinement in algorithms to remove PV artifact and to more accurately convert relaxivity to tracer concentration, coupled with improved AIF morphology achievable with multiecho and/or parallel sequences, may further improve quantitative DSC CBF measurements.

Acknowledgments

This work was supported in part by the NIH (2R01EB002711, 1R21EB006860, P41RR09784, K23NS051372) the Lucas foundation, and the Oak foundation.

References

1. Latchaw RE, Yonas H, Hunter GJ, et al. Guidelines and recommendations for perfusion imaging in cerebral ischemia. A scientific statement for healthcare professionals by the Writing Group on Perfusion Imaging, from the Council on Cardiovascular Radiology of the American Heart Association. Stroke. 2003; 34:1084–1104. [PubMed: 12677088]
2. Wintermark M, Sesay M, Barbier E, et al. Comparative overview of brain perfusion imaging techniques. Stroke. 2005; 36(9):e83–99. [PubMed: 16100027]
3. Østergaard L, Weisskoff RM, Chesler DA, Gyldensted C, Rosen BR. High resolution measurement of cerebral blood flow using intravascular tracer bolus passages. Part I: Mathematical approach and statistical analysis. Magn Reson Med. 1996; 36(5):715–725. [PubMed: 8916022]
4. Ostergaard L, Johannsen P, Host-Poulsen P, et al. Cerebral blood flow measurements by magnetic resonance imaging bolus tracking: comparison with [(15)O]H2O positron emission tomography in humans. J Cereb Blood Flow Metab. 1998; 18(9):935–940. [PubMed: 9740096]
5. Lin W, Celik A, Derdeyn C, et al. Quantitative measurements of cerebral blood flow in patients with unilateral carotid artery occlusion: a PET and MR study. J Magn Reson Imaging. 2001; 14(6):659–667. [PubMed: 11747021]
6. Mukherjee P, Kang HC, Videen TO, McKinstry RC, Powers WJ, Derdeyn CP. Measurement of cerebral blood flow in chronic carotid occlusive disease: comparison of dynamic susceptibility contrast perfusion MR imaging with positron emission tomography. AJNR Am J Neuroradiol. 2003; 24(5):862–871. [PubMed: 12748086]
7. Takasawa M, Jones PS, Guadagno JV, et al. How reliable is perfusion MR in acute stroke? Validation and determination of the penumbra threshold against quantitative PET. Stroke. 2008; 39(3):870–877. [PubMed: 18258831]
8. Carroll TJ, Teneggi V, Jobin M, et al. Absolute quantification of cerebral blood flow with magnetic resonance, reproducibility of the method, and comparison with H2(15)O positron emission tomography. J Cereb Blood Flow Metab. 2002; 22(9):1149–1156. [PubMed: 12218421]
9. Hagen T, Bartylla K, Piepgras U. Correlation of regional cerebral blood flow measured by stable xenon CT and perfusion MRI. J Comput Assist Tomogr. 1999; 23(2):257–264. [PubMed: 10096334]
10. Grandin CB, Bol A, Smith AM, Michel C, Cosnard G. Absolute CBF and CBV measurements by MRI bolus tracking before and after acetazolamide challenge: repeatabilily and comparison with PET in humans. Neuroimage. 2005; 26(2):525–535. [PubMed: 15907309]
11. Yonas H, Pindzola RR, Meltzer CC, Sasser H. Qualitative versus quantitative assessment of cerebrovascular reserves. Neurosurgery. 1998; 42(5):1005–1010. discussion 1011-1002. [PubMed: 9588544]

NIH-PA Author Manuscript

NIH-PA Author Manuscript

NIH-PA Author Manuscript

12. Calamante F, Vonken EJ, van Osch MJ. Contrast agent concentration measurements affecting quantification of bolus-tracking perfusion MRI. Magn Reson Med. 2007; 58(3):544–553. [PubMed: 17763347]
13. van Osch MJ, Vonken EJ, Viergever MA, van der Grond J, Bakker CJ. Measuring the arterial input function with gradient echo sequences. Magn Reson Med. 2003; 49(6):1067–1076. [PubMed: 12768585]
14. van Osch MJ, van der Grond J, Bakker CJ. Partial volume effects on arterial input functions: shape and amplitude distortions and their correction. J Magn Reson Imaging. 2005; 22(6):704–709. [PubMed: 16261570]
15. Kiselev VG. On the theoretical basis of perfusion measurements by dynamic susceptibility contrast MRI. Magn Reson Med. 2001; 46(6):1113–1122. [PubMed: 11746577]
16. Kjolby BF, Ostergaard L, Kiselev VG. Theoretical model of intravascular paramagnetic tracers effect on tissue relaxation. Magn Reson Med. 2006; 56(1):187–197. [PubMed: 16724299]
17. Jochimsen TH, Newbould RD, Skare ST, et al. Identifying systematic errors in quantitative dynamic-susceptibility contrast perfusion imaging by high-resolution multi-echo parallel EPI. NMR in biomedicine. 2007; 20(4):429–438. [PubMed: 17044140]
18. Johnson DW, Stringer WA, Marks MP, Yonas H, Good WF, Gur D. Stable xenon CT cerebral blood flow imaging: rationale for and role in clinical decision making. AJNR Am J Neuroradiol. 1991; 12(2):201–213. [PubMed: 1902015]
19. Wu O, Ostergaard L, Weisskoff RM, Benner T, Rosen BR, Sorensen AG. Tracer arrival timing-insensitive technique for estimating flow in MR perfusion-weighted imaging using singular value decomposition with a block-circulant deconvolution matrix. Magn Reson Med. 2003; 50(1):164–174. [PubMed: 12815691]
20. Mlynash M, Eyngorn I, Bammer R, Moseley M, Tong DC. Automated method for generating the arterial input function on perfusion-weighted MR imaging: validation in patients with stroke. AJNR Am J Neuroradiol. 2005; 26(6):1479–1486. [PubMed: 15956519]
21. Carroll TJ, Rowley HA, Haughton VM. Automatic calculation of the arterial input function for cerebral perfusion imaging with MR imaging. Radiology. 2003; 227(2):593–600. [PubMed: 12663823]
22. Østergaard L, Weisskoff RM, Chesler DA, Glydensted C, Rosen BR. High resolution measurement of cerebral blood flow using intravascular tracer passages. Part I: Mathematical approach and statistical analysis. Magn Reson Med. 1996; 36:715–725. [PubMed: 8916022]
23. Wu O, Ostergaard L, Koroshetz WJ, et al. Effects of tracer arrival time on flow estimates in MR perfusion-weighted imaging. Magn Reson Med. 2003; 50(4):856–864. [PubMed: 14523973]
24. Calamante F, Gadian DG, Connelly A. Delay and dispersion effects in dynamic susceptibility contrast MRI: simulations using singular value decomposition. Magn Reson Med. 2000; 44(3): 466–473. [PubMed: 10975900]
25. Lassen NA. Cerebral transit of an intravascular tracer may allow measurement of regional blood volume but not regional blood flow. J Cereb Blood Flow Metab. 1984; 4:633–634. [PubMed: 6501448]
26. Calamante F, Connelly A, van Osch MJ. Nonlinear DeltaR*2 effects in perfusion quantification using bolus-tracking MRI. Magn Reson Med. 2009; 61(2):486–492. [PubMed: 19161169]
27. Østergaard L, Smith DF, Vestergaard-Poulsen P, et al. Absolute cerebral blood flow and blood volume measured by magnetic resonance imaging bolus tracking: comparison with positron emission tomography values. J Cereb Blood Flow Metab. 1998; 18(4):425–432. [PubMed: 9538908]
28. Knutsson L, Borjesson S, Larsson EM, et al. Absolute quantification of cerebral blood flow in normal volunteers: correlation between Xe-133 SPECT and dynamic susceptibility contrast MRI. J Magn Reson Imaging. 2007; 26(4):913–920. [PubMed: 17896379]
29. Rempp KA, Brix G, Wenz F, Becker CR, Guckel F, Lorenz WJ. Quantitation of cerebral blood flow and volume with dynamic susceptibility contrast-enhanced MR imaging. Radiology. 1994; 193:637–641. [PubMed: 7972800]

NIH-PA Author Manuscript

NIH-PA Author Manuscript

NIH-PA Author Manuscript

30. Vonken EJ, van Osch MJ, Bakker CJ, Viergever MA. Measurement of cerebral perfusion with dual-echo multi-slice quantitative dynamic susceptibility contrast MRI. J Magn Reson Imaging. 1999; 10(2):109–117. [PubMed: 10441012]

31. Bleeker EJ, van Buchem MA, van Osch MJ. Optimal location for arterial input function measurements near the middle cerebral artery in first-pass perfusion MRI. J Cereb Blood Flow Metab. 2009; 29(4):840–852. [PubMed: 19142193]

32. Kjolby BF, Mikkelsen IK, Pedersen M, Ostergaard L, Kiselev VG. Analysis of partial volume effects on arterial input functions using gradient echo: a simulation study. Magn Reson Med. 2009; 61(6):1300–1309. [PubMed: 19365857]

33. Newbould RD, Skare ST, Jochimsen TH, et al. Perfusion mapping with multiecho multishot parallel imaging EPI. Magn Reson Med. 2007; 58(1):70–81. [PubMed: 17659630]

34. Calamante F, Morup M, Hansen LK. Defining a local arterial input function for perfusion MRI using independent component analysis. Magn Reson Med. 2004; 52(4):789–797. [PubMed: 15389944]

35. Gur D, Good WF, Wolfson SK Jr, Yonas H, Shabason L. Local cerebral blood flow measured by xenon-enhanced CT. Science. 1982; 215:1267–1268. [PubMed: 7058347]

36. Kishore PR, Rao GU, Fernandez RE, et al. Regional cerebral blood flow measurements using stable xenon enhanced computed tomography: a theoretical and experimental evaluation. J Comput Assist Tomogr. 1984; 8(4):619–630. [PubMed: 6736359]

NIH-PA Author Manuscript
NIH-PA Author Manuscript
NIH-PA Author Manuscript

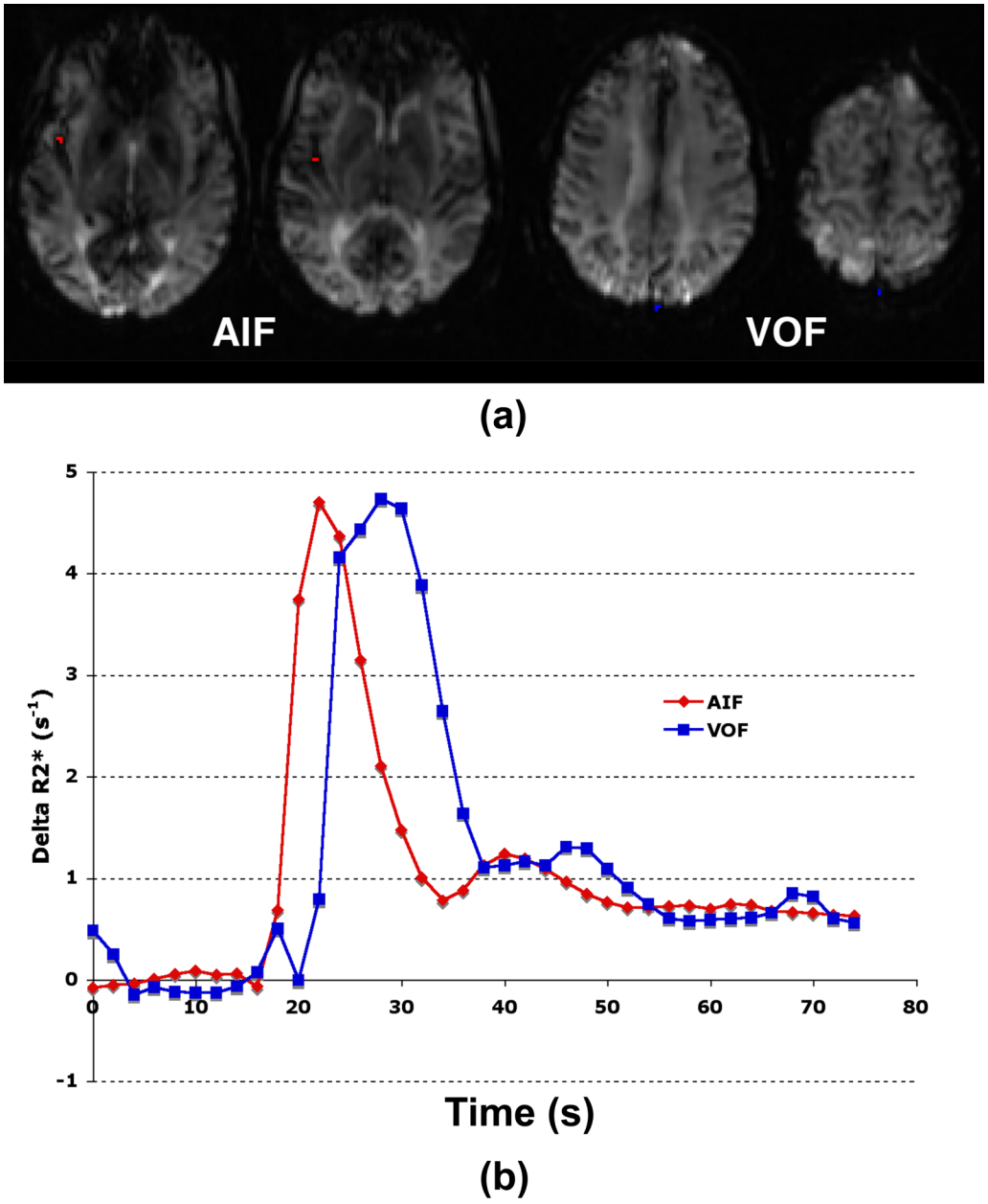

Figure 1.
(a) Example of the automated selection of AIF (red) and VOF (blue). Only 4 of 12 slices are shown, as these were the locations of the chosen AIF and VOF. (b) Concentration versus time curves. In this particular patient, the amount of AIF partial volume as calculated by the ratio of the areas-under-the-curve was 0.88.

NIH-PA Author Manuscript
NIH-PA Author Manuscript
NIH-PA Author Manuscript

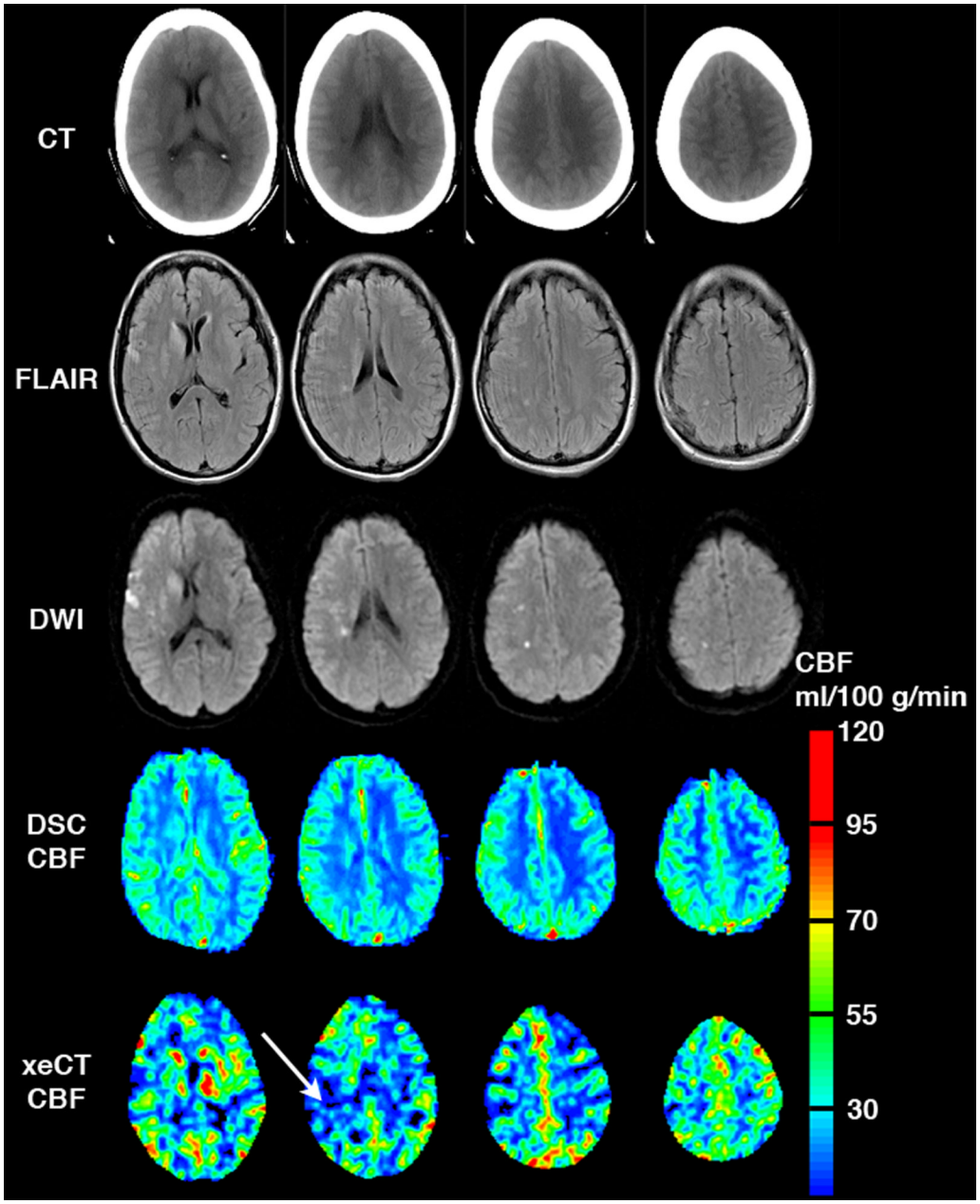

Figure 2.
Example of a typical co-registered data set, including CT, FLAIR, DWI, DSC CBF map, and xeCT CBF map. The DSC CBF map shown here is corrected for BB, but not for PV artifact (as this minimized bias and allows the images to be viewed on the same color scale more easily). The high signal on DWI represents acute cerebral ischemia. High CBF signal on the DSC map presumably represents artifact from large vessels, and partially obscures an area of low CBF on the xeCT study (arrow).

Figure 3.
Typical correlation of individual ROIs (1 cm^3 each) between DSC MRI and xeCT CBF, following correction for partial volume and bulk blood relaxivity. The slopes, intercepts, and correlation coefficients varied widely between patients (Table 2).

NIH-PA Author Manuscript
NIH-PA Author Manuscript
NIH-PA Author Manuscript

NIH-PA Author Manuscript
NIH-PA Author Manuscript
NIH-PA Author Manuscript

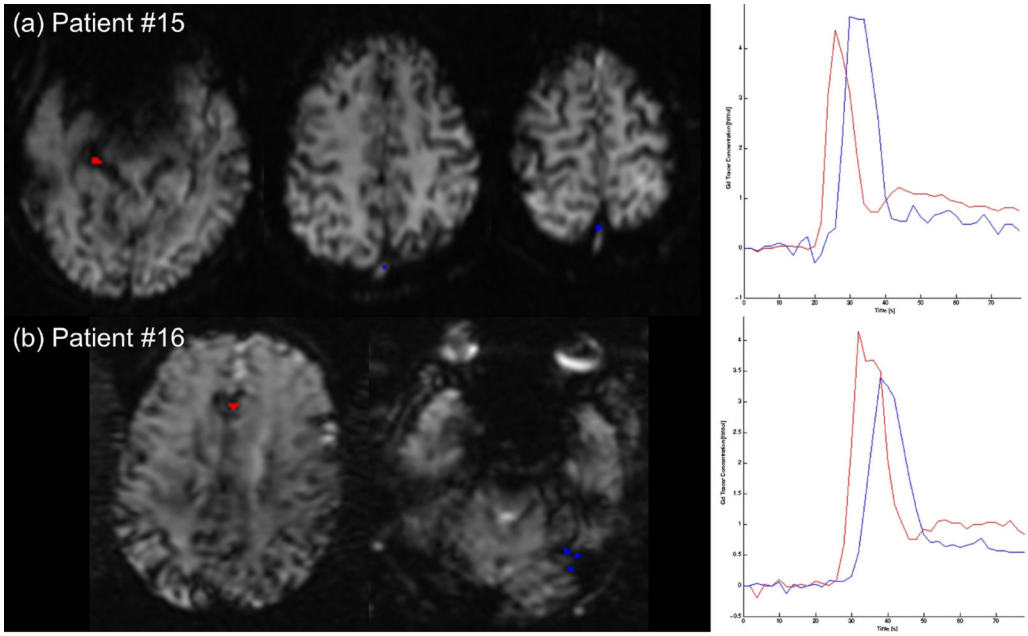

Figure 4.
In 2 of 18 cases (11%), the calculated AIF partial volume exceeded 1. (a) Patient #15: The AIF was selected in the right PCA, and the VOF in the superior sagittal sinus. The VOF shows some evidence of clipping, and the post-bolus baseline of the AIF is higher than the VOF, possibly due to contamination with venous structures in this region. (b) Patient #16: The AIF was selected in the ACA region, and the VOF in the region of the sigmoid/ transverse sinus. Here the VOF is slightly lower than expected, and the AIF post-bolus baseline again exceeds the VOF.

NIH-PA Author Manuscript
NIH-PA Author Manuscript
NIH-PA Author Manuscript

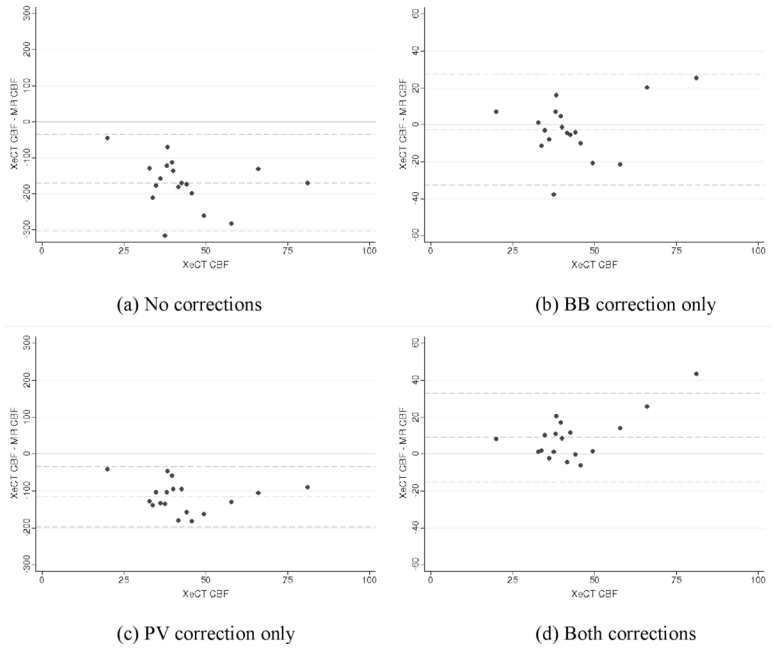

Figure 5.

Bland-Altman analysis of the difference in CBF as measured by MRI and xeCT plotted against the gold-standard xeCT CBF measurements for each of the four MRI post-processing conditions: (a) No correction, (b) BB correction only, (c) PV correction only, and (d) both corrections. Dotted lines represent the mean difference and the 95% limits of agreement. Note that the BB correction decreases MRI- based CBF measurements significantly, such that measured values (both with and without PV correction) are of the same order of magnitude as the xeCT CBF.

NIH-PA Author Manuscript

NIH-PA Author Manuscript

NIH-PA Author Manuscript

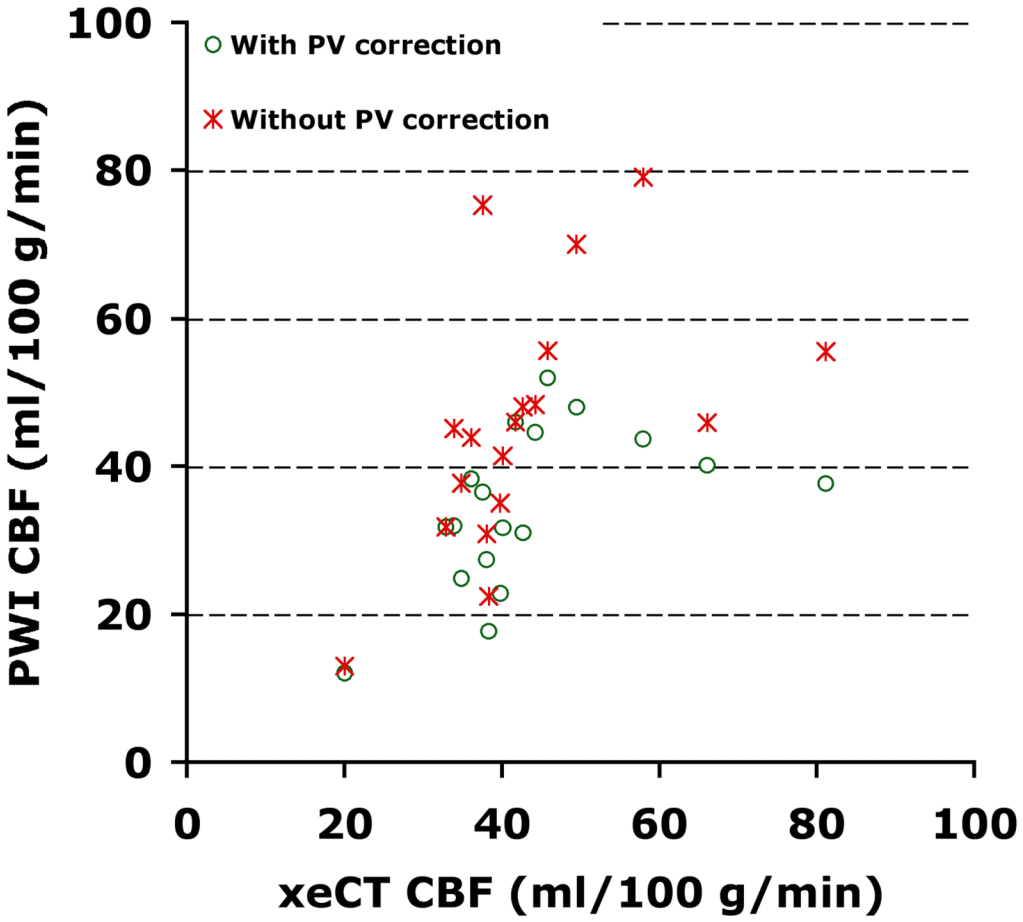

Figure 6.
Plot of global MRI-based CBF measurement versus gold-standard xeCT CBF with and without partial volume correction. Both MRI-based measurements have been corrected for the quadratic relationship between contrast relaxivity and concentration. As can be seen, the PV correction results in a consistent reduction in the measured CBF.

NIH-PA Author Manuscript
NIH-PA Author Manuscript
NIH-PA Author Manuscript

Table 1

Patient demographics

Pt	Age/Gender	Symptoms/Indication	Imaging Findings
1	51/F	Transient expressive aphasia, s/p L ICA angioplasty 8 mos ago	L cavernous ICA 80% stenosis R cavernous ICA 70% stenosis, R parietal chronic infarct
2	38/F	L-sided weakness 1 month prior with known R basal ganglia infarct	Subacute R basal ganglia infarct, R M1 75% stenosis
3	40/F	Transient L-sided hemiparesis, R-sided neck pain	R proximal ICA occlusion (dissection), multiple embolic acute infarcts R MCA territory
4	63/F	Transient R-sided weakness and numbness, hypertension	L M1 stenosis 80%, no acute infarct
5	28/M	Transient R-sided symptoms, ankylosing spondylitis	R supraclinoid ICA high-grade stenosis with M1 reconstitution.
6	19/M	R-sided weakness, dysarthria, subacute bacterial endocarditis	L MCA acute embolic infarct, L posterior M2 occlusion
7	56/M	R upper extremity weakness/poor coordination & aphasia	L MCA acute embolic infarct, L ICA occlusion, R ICA 40% stenosis
8	47/M	R-sided weakness, slurred speech, headache 13 days prior	L MCA acute/subacute infarct, L ICA occlusion (dissection), R ICA 40% stenosis
9	48/M	3 wks s/p acute confusion, dyscalcula, dysarthria, dizziness	B borderzone acute infarcts, B ICA occlusion
10	43/F	1 wk s/p anterior communicating aneurysm coiling, evaluated for ischemia due to vasospasm	Tiny punctate subacute infarcts frontal lobe, symmetric perfusion, artifact from coiling
11	87/M	R-sided facial droop and hemiparesis 4 days prior	Small punctate watershed L MCA-ACA subacute infarct. L M1 MCA high-grade stenosis
12	47/F	6 mos s/p R STA-MCA bypass for Moyamoya disease, asymptomatic	B supraclinoid ICA occlusion. Patent R STA-MCA bypass. No acute infarcts. Chronic B MCA-ACA borderzone infarcts
13	28/F	Pre-operative evaluation for B Moyamoya disease, s/p recent strokes	L supraclinoid ICA occlusion. R supraclinoid ICA and M1 high grade stenosis. No acute infarcts. Several old R MCA-ACA borderzone infarcts
14	40/M	Moyamoya disease s/p L STA-MCA bypass with new visual field cut	No acute infarct and unchanged L supraclinoid high grade stenosis
15	31/F	Moyamoya disease, 6 months s/p bilateral STA-MCA bypass	No acute infarcts, patent bypass grafts
16	73/M	Acute onset left hemiparesis, 4 days prior	Acute infarct in the right basal ganglia and frontal operculum R ICA occlusion
17	54/F	Moyamoya disease, 6 months s/p bilateral STA-MCA bypass	No acute infarcts, patent bypass grafts. Old R parieto-occipital infarct
18	45/M	Aphasia and R facial numbness 1 month ago	Punctate tiny acute infarcts in the L corona radiata Chronic borderzone infarcts. L ICA occlusion. R ICA high-grade stenosis
	Mean±SD 47±17 yrs 9 M, 9 F		6 unilateral ICA occlusion, 2 bilateral ICA occlusion

L: left; R: right; B: bilateral; ICA: internal carotid artery; MCA: middle cerebral artery; M1: 1st segment of the middle cerebral artery; ACA: anterior cerebral artery; STA: superficial temporal artery.

NIH-PA Author Manuscript
NIH-PA Author Manuscript
NIH-PA Author Manuscript

Table 2

Correlation of DSC and xeCT CBF in individual patients

	Without BB correction			With BB correction		
	Slope	**Intercept**	**R**	**Slope**	**Intercept**	**R**
Patient #						
1	1.12	122.8	0.39	0.29	26.8	0.39
2	1.55	113.3	0.43	0.35	23.5	0.42
3	1.00	103.9	0.43	0.18	18.5	0.40
4	1.51	71.0	0.43	0.39	14.5	0.40
5	2.36	95.6	0.64	0.66	15.6	0.62
6	1.52	46.8	0.48	0.37	7.4	0.47
7	0.42	119.1	0.15	0.09	27.1	0.15
8	0.77	140.4	0.22	0.19	31.5	0.21
9	2.21	97.6	0.54	0.43	17.3	0.50
10	1.78	145.7	0.54	0.53	27.8	0.55
11	0.90	42.4	0.30	0.17	8.6	0.29
12	1.83	71.5	0.50	0.36	13.9	0.49
13	1.29	35.8	0.55	0.26	7.6	0.54
14	0.33	85.8	0.18	0.07	19.8	0.18
15	1.44	161.9	0.26	0.29	33.8	0.26
16	1.25	119.6	0.26	0.25	23.5	0.26
17	2.10	50.2	0.60	0.50	11.8	0.60
18	2.31	98.4	0.54	0.51	22.1	0.53
Totals	1.43±0.61	95.7±37.0	0.41±0.15	0.33±0.16	19.5±8.1	0.40±0.15

Data shown is for PV corrected CBF maps. The correlations did not change based on PV correction, as this was a global scaling factor for each patient. After BB correction, it should be noted that the slope is less than 1 and the intercept is greater than 0 ($p<0.05$).

NIH-PA Author Manuscript

NIH-PA Author Manuscript

NIH-PA Author Manuscript

Table 3

Effects of partial volume and nonlinear contrast relaxivity correction on MRI-based DSC CBF maps.

Correction method		Bulk blood correction	
		No	Yes
Partial volume correction	No	CBF 211.9±73.9	CBF 45.8±17.2
		CBF Ratio 5.01±1.65	CBF Ratio 1.07±0.34
		COV 33%	COV 32%
		R=0.45, p=0.06	R=0.53, p=0.02
	Yes	CBF 158.9±45.6	CBF 34.3±10.8
		CBF Ratio 3.79±1.05	CBF Ratio 0.81±0.22
		COV 28%	COV 27%
		R=0.42, p=0.08	R=0.52, p=0.02
xeCT (gold standard)	CBF 43.3±13.7		

All measurements mean±SD. CBF results are in ml/100 g/min. COV = coefficient of variation, or the between-patients standard deviation of the CBF ratio normalized by the mean, which is a marker of precision (see Eq 4). R was determined using the simple Pearson correlation between the two measurements.